Nuclear reaction cross sections of exotic nuclei in the Glauber model for relativistic mean field densities

S. K. Patra,[1] R. N. Panda,[2] P. Arumugam,[3] and Raj K. Gupta[4]
[1]*Institute of Physics, Sachivalaya Marg, Bhubaneswar-751 005, India*
[2]*Department of Physics, ITER, Siksha 'O' Anusandhan University, Bhubaneswar-751 030, India*
[3]*Department of Physics, Indian Institute of Technology, Roorkee-247 667, India*
[4]*Department of Physics, Panjab University, Chandigarh-160 014, India*
(Received 3 July 2009; revised manuscript received 12 September 2009; published 2 December 2009)

We have calculated the total nuclear reaction cross sections of exotic nuclei in the framework of the Glauber model, using as inputs the standard relativistic mean field (RMF) densities and the densities obtained from the more recently developed effective-field-theory-motivated RMF (the E-RMF). Both light and heavy nuclei are taken as the representative targets, and the light neutron-rich nuclei as projectiles. We found the total nuclear reaction cross section to increase as a function of the mass number, for both the target and projectile nuclei. The differential nuclear elastic scattering cross sections are evaluated for some selected systems at various incident energies. We found a large dependence of the differential elastic scattering cross section on incident energy. Finally, we have applied the same formalism to calculate both the total nuclear reaction cross section and the differential nuclear elastic scattering cross section for the recently discussed superheavy nucleus with atomic number $Z = 122$.

DOI: 10.1103/PhysRevC.80.064602 PACS number(s): 21.10.Dr, 24.10.Eq, 24.10.Jv, 25.60.Dz

I. INTRODUCTION

Study of unstable nuclei with radioactive ion beam (RIB) facilities has opened up an exciting new channel to look for some crucial issues in the context of both nuclear structure and nuclear astrophysics [1,2]. Unstable nuclei play an important, and in some cases dominant, role in many phenomena in the cosmos such as novae, supernovae, x-ray and γ-ray bursts (GRBs), and other stellar explosions. A recent work [3] shows that in relativistic jets of GRBs or supernovae jets near the nascent neutron star, the formation of ultra-neutron-rich and superheavy nuclei is possible. The sources of the formation of these nuclei are the nuclear reactions and fusion phenomena in the cosmological objects.

The direct study of stellar properties in ground-based laboratories has become more attractive, thanks to the availability of RIBs; for example, the study of the ^{18}Ne-induced neutron pickup reaction could reveal information about the exotic $^{15}\mathrm{O} + {}^{19}\mathrm{Ne}$ reaction, happening in the CNO cycle in burning stars. Study of the structure and reactions of unstable nuclei is therefore required in order to improve our understanding of the astrophysical origin of atomic nuclei and the evolution of stars and their (sometimes explosive) death. Recently, Satpathy *et al.* [4] reported that the neutron-rich U and Th isotopes are thermally fissile and could release an order of magnitude more energy than ^{235}U fission in a new fission-decay mode, called multifragmentation fission, which happened often in astrophysical objects. The possible formation of these highly neutron-rich nuclei and the recent report on the possible discovery of $^{292}X_{122}$ nucleus [5] in a chemical process motivated us to study the nuclear reaction properties of some highly neutron-rich targets as well as the projectiles.

The secondary radioactive beam technique is useful in studying the various nuclear reaction cross sections, such as the total reaction cross sections, differential elastic scattering cross sections, and Coulomb breakup cross sections. Study of these quantities enables us to know the nuclear structure of unstable nuclei in detail, particularly the halo structure near the drip lines [6–9]. This will also help in studying the formation of neutron-rich nuclei that are surrounded by a high pressure or temperature. Thus, the total nuclear reaction cross section, both for proton-nucleus and nucleus-nucleus scattering, has been a subject of interest for the last few decades [10–13]. The main objective of the present work is to study the total nuclear reaction cross sections of exotic nuclei using the densities obtained from relativistic mean field (RMF) and field-theory-motivated effective Lagrangian (E-RMF) approaches in conjunction with the Glauber model.

The paper is designed as follows. The RMF and E-RMF formalisms, used in the calculations of density profiles, are explained briefly in Sec. II. The reaction formalism in the framework of the Glauber model is also explained in that section. The results obtained from our calculations using both the RMF and E-RMF densities are discussed in Sec. III. The ground-state properties of finite drip line and heavy nuclei, which are relevant for the present study, are also presented here. Applications are also made to the recently observed superheavy element $Z = 122$ [5]. Finally, a brief summary and concluding remarks are given in Sec. IV.

II. THEORETICAL FRAMEWORK

A. RMF and E-RMF formalisms

The use of RMF and E-RMF formalisms on finite nuclei as well as on infinite nuclear matter is well documented and details can be found in Ref. [14] for the RMF theory and in Refs. [8,15] for the recent extension of RMF formalism to the field-theory-motivated effective Lagrangian approach,

the E-RMF. Here, we present only some very essential steps needed for the present paper. As already mentioned above, we need the RMF and E-RMF density profiles for our calculations of the total reaction as well as the differential elastic scattering cross sections. The energy density functional of the E-RMF model for finite nuclei is written as [16,17]

$$\begin{aligned}\mathcal{E}(\mathbf{r}) = \sum_{\alpha}\varphi_{\alpha}^{\dagger}\Bigg\{&-i\boldsymbol{\alpha}\cdot\nabla+\beta(M-\Phi)+W+\frac{1}{2}\tau_3 R\\&+\frac{1+\tau_3}{2}A-\frac{i}{2M}\beta\boldsymbol{\alpha}\cdot\left(f_v\nabla W+\frac{1}{2}f_\rho\tau_3\nabla R+\lambda\nabla A\right)\\&+\frac{1}{2M^2}\left(\beta_s+\beta_v\tau_3\right)\Delta A\Bigg\}\varphi_{\alpha}\\&+\left(\frac{1}{2}+\frac{\kappa_3}{3!}\frac{\Phi}{M}+\frac{\kappa_4}{4!}\frac{\Phi^2}{M^2}\right)\frac{m_s^2}{g_s^2}\Phi^2-\frac{\zeta_0}{4!}\frac{1}{g_v^2}W^4\\&+\frac{1}{2g_s^2}\left(1+\alpha_1\frac{\Phi}{M}\right)(\nabla\Phi)^2-\frac{1}{2g_v^2}\left(1+\alpha_2\frac{\Phi}{M}\right)\\&\times(\nabla W)^2-\frac{1}{2}\left(1+\eta_1\frac{\Phi}{M}+\frac{\eta_2}{2}\frac{\Phi^2}{M^2}\right)\frac{{m_v}^2}{{g_v}^2}W^2\\&-\frac{1}{2g_\rho^2}(\nabla R)^2-\frac{1}{2}\left(1+\eta_\rho\frac{\Phi}{M}\right)\frac{m_\rho^2}{g_\rho^2}R^2\\&-\frac{1}{2e^2}(\nabla A)^2+\frac{1}{3g_\gamma g_v}A\Delta W+\frac{1}{g_\gamma g_\rho}A\Delta R,\end{aligned}\tag{1}$$

where the index α runs over all occupied states $\varphi_\alpha(\mathbf{r})$ of the positive energy spectrum, $\Phi \equiv g_s\phi_0(\mathbf{r})$, $W \equiv g_v V_0(\mathbf{r})$, $R \equiv g_\rho b_0(\mathbf{r})$, and $A \equiv eA_0(\mathbf{r})$.

The terms with g_γ, λ, β_s, and β_v take care of the effects related to the electromagnetic structure of the pion and the nucleon (see Ref. [17]). Specifically, the constant g_γ concerns the coupling of the photon to the pions and the nucleons through the exchange of neutral vector mesons. The experimental value is $g_\gamma^2/4\pi = 2.0$. The constant λ is needed to reproduce the magnetic moments of the nucleons and is defined by

$$\lambda = \tfrac{1}{2}\lambda_p(1+\tau_3)+\tfrac{1}{2}\lambda_n(1-\tau_3),\tag{2}$$

with $\lambda_p = 1.793$ and $\lambda_n = -1.913$, the anomalous magnetic moments of the proton and the neutron, respectively. The terms with β_s and β_v contribute to the charge radii of the nucleon [17].

The energy density contains tensor couplings and scalar-vector and vector-vector meson interactions, in addition to the standard scalar self-interactions κ_3 and κ_4. The E-RMF formalism can be interpreted as a covariant formulation of density functional theory as it contains all the higher order terms in the Lagrangian, obtained by expanding it in powers of the meson fields. The terms in the Lagrangian are kept finite by adjusting the parameters. Further insight into the concepts of the E-RMF model can be obtained from Ref. [17]. It may be noted that the standard RMF Lagrangian is obtained from that of the E-RMF by ignoring the vector-vector and scalar-vector cross interactions, and hence does not need a separate discussion.

In each of the two formalisms (E-RMF and RMF), the set of coupled equations are solved numerically by a self-consistent iteration method. The baryon, scalar, isovector, proton, and tensor densities are

$$\rho(r) = \sum_{\alpha}\varphi_{\alpha}^{\dagger}(r)\varphi_{\alpha}(r),\tag{3}$$

$$\rho_s(r) = \sum_{\alpha}\varphi_{\alpha}^{\dagger}(r)\beta\varphi_{\alpha}(r),\tag{4}$$

$$\rho_3(r) = \sum_{\alpha}\varphi_{\alpha}^{\dagger}(r)\tau_3\varphi_{\alpha}(r),\tag{5}$$

$$\rho_{\mathrm{p}}(r) = \sum_{\alpha}\varphi_{\alpha}^{\dagger}(r)\left(\frac{1+\tau_3}{2}\right)\varphi_{\alpha}(r),\tag{6}$$

$$\rho_{\mathrm{T}}(r) = \sum_{\alpha}\frac{i}{M}\nabla\cdot[\varphi_{\alpha}^{\dagger}(r)\beta\boldsymbol{\alpha}\varphi_{\alpha}(r)],\tag{7}$$

$$\rho_{\mathrm{T},3}(r) = \sum_{\alpha}\frac{i}{M}\nabla\cdot[\varphi_{\alpha}^{\dagger}(r)\beta\boldsymbol{\alpha}\tau_3\varphi_{\alpha}(r)].\tag{8}$$

For the detailed field equations and numerical procedure for calculating the ground-state properties of finite nuclei, we refer the reader to Refs. [14,15]. The densities, obtained from the RMF and E-RMF formalisms, respectively, with NL3 [18] and G2 [8] parametrizations, are used in the formalism of the Glauber model for getting the total nuclear reaction and differential elastic scattering cross sections.

B. Glauber model and total nuclear reaction cross section

The theoretical formalism to calculate the total nuclear reaction cross section, using the Glauber approach, has been given by R. J. Glauber [19]. The Glauber model is based on the independent, individual nucleon-nucleon (NN) collisions in the overlap zone of the colliding nuclei, and has been used extensively to explain the observed total nuclear reaction cross sections for various systems at high energies. The standard Glauber form for the total reaction cross section at high energies is expressed as [19]

$$\sigma_r = 2\pi\int_0^{\infty} b[1-T(b)]\,db,\tag{9}$$

where $T(b)$, the transparency function, is the probability that, at an impact parameter b, the projectile passes through the target without interacting. The function $T(b)$ is calculated in the overlap region between the projectile and the target, where the interactions are assumed to result from a single NN collision, and is given by

$$T(b) = \exp\left[-\sum_{i,j}\overline{\sigma}_{ij}\int d\vec{s}\,\overline{\rho}_{ti}(s)\,\overline{\rho}_{pj}(|\vec{b}-\vec{s}|s)\right].\tag{10}$$

Here, the summation indices i and j run over the proton and neutron, and subscripts p and t refer to projectile and target, respectively. $\overline{\sigma}_{ij}$ is the experimental nucleon-nucleon reaction cross section which varies with energy. The z-integrated densities $\overline{\rho}(\omega)$ are defined as

$$\overline{\rho}(\omega) = \int_{-\infty}^{\infty}\rho(\sqrt{\omega^2+z^2})\,dz,\tag{11}$$

with $\omega^2 = x^2 + y^2$. The argument of $T(b)$ in Eq. (10) is $|\vec{b} - \vec{s}|$, which stands for the impact parameter between the ith and jth nucleons.

Initially, the Glauber model was indeed designed for high-energy approximation. However, it was found to work fairly well, for both the nucleus-nucleus reaction cross sections and the differential elastic scattering cross sections, over a broad energy range [20]; i.e., the model reproduced the results at incident energies of 25, 30, and 85 MeV/nucleon. Thus, for including the low-energy effects of increasing the NN interaction, the above-stated original Glauber model is modified to take care of the finite range effects [21,22] in profile function and the Coulomb modified trajectories. Thus, for the finite range approximation, the transparency function is given by [21,23]

$$T(b) = \exp\left[-\int_{P,T}\sum_{i,j}[\Gamma_{ij}(\vec{b}-\vec{s}+\vec{t})]\overline{\rho}_{Pi}(\vec{t})\overline{\rho}_{Tj}(\vec{s})d\vec{s}\,d\vec{t}\right], \tag{12}$$

the summation indices i and j run over neutron and proton for both target and projectile. Here the profile function Γ_{ij} is

$$\Gamma_{ij}(b_{\rm eff}) = \frac{1 - i\alpha_{NN}}{2\pi\beta_{NN}^2}\sigma_{NN}\exp\left(-\frac{b_{\rm eff}^2}{2\beta_{NN}^2}\right), \tag{13}$$

with $b_{\rm eff} = |\vec{b} - \vec{s} + \vec{t}|$, $\vec{b}$ being the impact parameter, and $\vec{s}$ and $\vec{t}$ are just the dummy variables for integration over the z-integrated target and projectile densities. The parameters σ_{NN}, α_{NN}, and β_{NN} are usually case dependent (proton-proton, neutron-neutron, or proton-neutron), but we have used here the appropriate average values from Ref. [24].

The nuclear densities, obtained from the RMF or E-RMF models, are fitted to a sum of two Gaussian functions, with appropriate coefficients c_i and ranges a_i chosen for the respective nuclei, as

$$\rho(r) = \sum_{i=1}^{N} c_i \exp[-a_i r^2]. \tag{14}$$

Then, the Glauber model is used to calculate the total reaction cross section for both the stable and unstable nuclei.

C. Differential elastic scattering cross section

The differential elastic scattering cross section, in terms of the differential Rutherford scattering cross section $(\frac{d\sigma}{d\Omega})_r$, is given by

$$\frac{d\sigma}{d\Omega} = \left(\frac{d\sigma}{d\Omega}\right)\Big/\left(\frac{d\sigma}{d\Omega}\right)_r = \frac{|F(\mathbf{q})|^2}{|F_{\rm Coul}(\mathbf{q})|^2}. \tag{15}$$

$F(\mathbf{q})$ and $F_{\rm Coul}(\mathbf{q})$ are the elastic and Coulomb (elastic) scattering amplitudes, respectively.

The elastic scattering amplitude $F(\mathbf{q})$ is written as

$$F(\mathbf{q}) = e^{i\chi_s}\left\{F_{\rm Coul}(\mathbf{q}) + \frac{iK}{2\pi}\int dbe^{-iq.b+2i\eta\ ln(Kb)}T(b)\right\} \tag{16}$$

with the Coulomb elastic scattering amplitude $F_{\rm Coul}(\mathbf{q})$ given as

$$F_{\rm Coul}(\mathbf{q}) = \frac{-2\eta K}{q^2}\exp\left\{-2i\eta\ ln\left(\frac{q}{2K}\right) + 2i\arg\Gamma(1+i\eta)\right\}. \tag{17}$$

Here $\eta = Z_P Z_T e^2/\hbar v$ is the Sommerfeld parameter, v the incident velocity, and $\chi_s = -2\eta\ln(2Ka)$, with a being the screening radius [19]. The differential elastic scattering cross section does not depend on the screening radius a.

III. RESULTS AND DISCUSSION

A. Ground-state properties of finite nuclei in RMF and E-RMF models

It is well known that the standard RMF model is a powerful formalism for calculating the ground-state properties of finite nuclei. This model is surprisingly successful for not only the nuclei near the valley of stability, but also the nuclei far away from the β-stability line [14]. On the other hand, the recently developed E-RMF formalism reproduces the properties of finite nuclei as well as with the RMF model, with the additional success of describing the properties of nuclear matter, including the properties of astrophysical objects such as a neutron star [8,9,15]. In standard RMF, with the NL3 parameter set, the nuclear matter compressibility $K_\infty \sim 271.5$ MeV [18], which is slightly more than the empirical value of $K_\infty = 210 \pm 30$ MeV [25]. It is around 215 MeV [8] in the E-RMF formalism, which is closer to the data.

In the calculation of the total nuclear reaction cross section, density is the input in the Glauber model. If we estimate nuclear radii properly, then our predictions of total reaction cross sections will be accurate. For this reason, first of all we have evaluated the ground-state binding energies, nuclear radii, densities, etc., using the RMF and E-RMF formalisms, which are given in Tables I and II and Figs. 1 and 2. In some of our earlier works [26], it was demonstrated that the total reaction cross section does not depend much on the deformation of reacting nuclei; therefore, in our present calculations, we proceed with spherical densities, i.e., without taking the deformation into account. For the choice of parameter set, although there exist a number of parameter sets for solving the standard RMF as well as E-RMF Lagrangians, we have employed here the most successful NL3 set for the former and G2 for the latter formalism.

1. Binding energies

We present in Tables I and II, the calculated binding energies, using the RMF and E-RMF formalisms with NL3 and G2 forces, respectively, for the light and heavy nuclei to be used as projectiles and targets in the following calculations of the reaction cross sections. The experimental data, taken from Ref. [27], are also given for comparison. It is evident from Tables I and II that both the calculated binding energies from RMF(NL3) and E-RMF(G2) models are similar

TABLE I. Binding energy (BE) in MeV, rms charge radius (r_c) in fm for light nuclei (used as projectiles) obtained from RMF(NL3) and E-RMF(G2) formalisms compared with experimental data.

Nucleus	BE			r_c		
	RMF	E-RMF	Expt. [27]	RMF	E-RMF	Expt. [Ref.]
^{4}He	28.14	29.39	28.30	2.063	2.076	1.676(8) [28]
^{5}He	28.32	29.87	27.41	2.054	2.045	
^{6}He	29.45	31.37	29.27	2.039	2.003	2.068(11) [28]
^{7}He	31.541	33.86	28.83	2.039	1.958	
^{8}He	34.55	37.27	31.41	2.011	1.912	1.929(26) [28]
^{6}Li	29.82	31.85	31.99	2.546	2.508	2.51(6) [29]
^{7}Li	34.04	36.47	39.24	2.375	2.345	2.39(3) [29]
^{8}Li	39.44	42.17	41.28	2.291	2.256	2.29(8) [29]
^{9}Li	45.83	48.75	45.34	2.239	2.195	2.22(9) [29]
^{10}Li	48.23	51.10	45.32	2.283	2.234	
^{11}Li	51.50	54.23	45.64	2.323	2.256	2.217(35) [30]
^{10}B	59.18	61.42	64.75	2.451	2.492	2.45(12) [31]
^{15}B	84.90	88.20	88.19	2.497	2.479	
^{17}B	85.57	90.13	89.52	2.524	2.456	
^{20}B	86.58	92.13		2.58	2.510	
^{12}C	88.21	87.22	92.16	2.363	2.497	2.44(2) [31]
^{14}C	104.32	105.49	105.28	2.506	2.539	2.56(5) [31]
^{16}C	106.50	108.93	110.75	2.525	2.531	
^{18}C	110.40	114.05	115.66	2.545	2.526	
^{20}C	115.93	120.73	119.18	2.566	2.522	

and coincide very well with the experimental data. A further inspection of the tables shows that for light nuclei (Table I), some of the RMF(NL3) results are slightly lower than the experimental values. On the other hand, the results predicted by the E-RMF(G2) overestimate the data, and vice versa for the heavier nuclei. We also know from the properties of the mean field formalism that it has some limitations for the light mass region of the periodic table, and hence the small discrepancies of RMF results with experimental data could be attributed to that fact. In any case, to get a qualitative estimation of the binding energy, the RMF as well as E-RMF results are trust worthy and can be used for further calculations in the chosen light mass region.

Our analysis of the binding energies for heavy mass nuclei, which we use here as the targets for nuclear reactions, shows that, except for ^{208}Pb, our results are a few MeV lower than the experimental data. Unlike the light mass region, the mean field approximation is extremely suited to the heavier mass region of the periodic table. However, although the mean field approximation is properly applicable for these heavy nuclei, these nuclei are well deformed, which is ignored here in our calculations. Hence, due to this simplification, we compromise a few MeV of binding energy in calculated values with experimental data, which does not affect the nuclear reaction cross sections, as reported in Ref. [26].

2. *Nuclear radii*

The rms charge radius r_c is obtained from the point proton rms radius through the relation [14] $r_c = \sqrt{r_p^2 + 0.64}$, where the factor 0.64 accounts for the finite size effects of protons with radius 0.8 fm. Tables I and II show the calculated nuclear charge radii r_c using RMF and E-RMF models together with the experimental data, wherever available. We notice from these tables that both models (RMF as well as E-RMF) give similar results for the rms charge radii and both account fairly

TABLE II. Same as Table I, but for heavy nuclei (used as targets).

Nucleus	BE			r_c		
	RMF	E-RMF	Expt. [27]	RMF	E-RMF	Expt. [Ref.]
^{208}Pb	1637.62	1631.80	1636.43	5.523	5.499	5.498(10) [31]
^{210}Pb	1644.22	1638.42		5.426	5.515	
^{218}Pb	1673.84	1667.87		5.623	5.583	
^{228}Pb	1709.10	1704.48		5.693	5.665	
^{238}Pb	1738.53	1735.89		5.754	5.733	
^{248}Pb	1765.68	1764.75		5.812	5.792	
^{258}Pb	1789.11	1790.21		5.868	5.848	
^{260}Pb	1792.76	1794.23		5.879	5.858	
^{230}Th	1732.77	1725.70	1755.13	5.739	5.711	
^{240}Th	1767.75	1763.49		5.800	5.777	
^{250}Th	1800.03	1797.75		5.859	5.838	
^{260}Th	1828.47	1827.94		5.913	5.891	
^{270}Th	1910.40	1906.78		6.007	5.982	
^{235}U	1778.65	1764.62	1783.86	5.833	5.813	
^{238}U	1793.50	1780.74	1801.69	5.851	5.830	5.8434 [31]
^{250}U	1850.67	1842.36		5.923	5.899	
^{260}U	1893.33	1887.37		5.982	5.959	
^{270}U	1930.71	1925.40		6.025	6.001	
^{280}U	1952.73	1947.30		6.087	6.053	
$^{292}X_{122}$	2037.34	2019.90		6.306	6.284	
$^{320}X_{122}$	2213.01	2195.90		6.477	6.453	

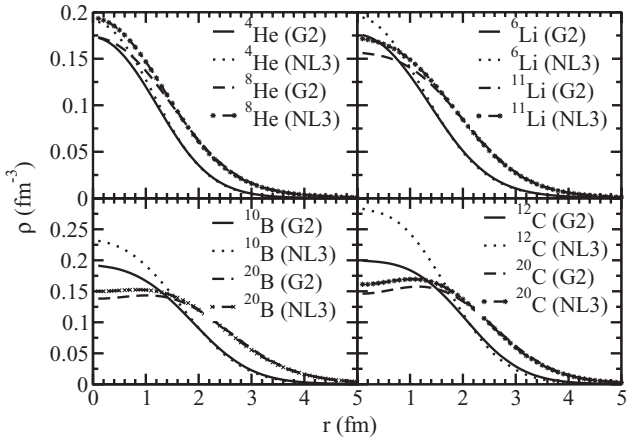

FIG. 1. Ground-state densities for some light nuclei (as projectiles) obtained from the RMF(NL3) and E-RMF(G2) formalisms.

well for the experimentally observed values. Since the charge radius is obtained from the density profile, and our RMF and E-RMF results for r_c match the experimental data rather well, we can reliably use these density profiles in the calculation of nuclear reaction cross sections, which is one of the main objective of the present study.

3. *Nuclear density*

The nuclear densities, obtained from Eq. (3), using both RMF(NL3) and E-RMF(G2) are plotted in Figs. 1 and 2. These are the most crucial and required quantities for our calculations of the total nuclear reaction cross sections using the Glauber model. Figure 1 depicts the densities for some representative light nuclei, to be used as projectiles in our calculations. We notice from Fig. 1 that the nuclear densities for RMF(NL3) and E-RMF(G2) for lighter nuclei are considerably different near the center of the nucleus. This difference reduces as we go away from the middle of the nuclei toward the surface. As expected, the density distribution is elongated for neutron-rich nuclei, as compared to the stable isotopes. All the pairs of nuclei (^{4}He, ^{8}He), (^{6}Li, ^{11}Li), (^{10}B, ^{20}B), and (^{12}C, ^{20}C) shown here present the same features for the light mass region.

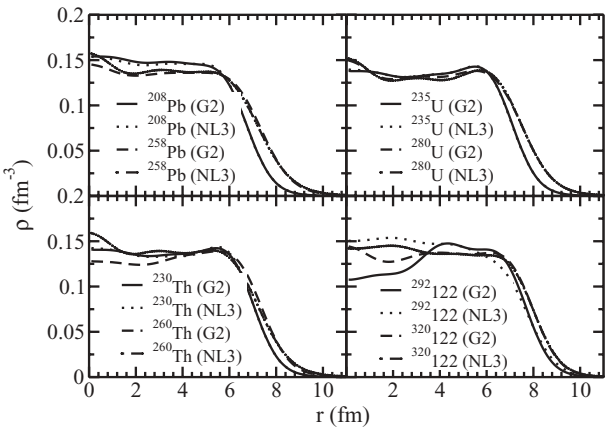

FIG. 2. Same as Fig. 1, but for heavy nuclei (as targets).

Similarly, in Fig. 2, we have shown the density distributions for pairs of heavy nuclei (^{208}Pb, ^{258}Pb), (^{235}U, ^{280}U), (^{230}Th, ^{260}Th), and the recent, possibly discovered, naturally occurring superheavy nucleus $^{292}X_{122}$ ($Z = 122$, $N = 170$) [5] and its neutron-rich isotope $^{320}X_{122}$. Unlike the light mass nuclei, densities obtained from RMF(NL3) and E-RMF(G2) in these pairs of heavy nuclei are not much different, even in the central region of the nucleus. Surprisingly, we find a deep minimum at the center in the density distribution for the $^{320}X_{122}$ nucleus, which is quite different from other densities obtained for normal nuclei shown in this figure. In the following, we use these, as well as some other densities, for the predictions of total nuclear reaction cross sections.

B. Coefficients of Gaussian functions fitted to mimic the density distributions, the input for the profile function

The nuclear densities obtained above from the RMF and E-RMF models for the projectile and target nuclei, which are the main ingredients of the calculation of total nuclear reaction cross sections, have been fitted to a sum of two Gaussians in Eq. (14), and the calculated coefficients c_1, c_2 and ranges a_1, a_2 are listed in Tables III and IV. This fitting procedure simplifies the numerical calculations considerably [32] and makes it possible to obtain analytic expressions for the transparency functions defined in Eqs. (10) and (12). In other words, using these coefficients [in Eq. (14)], we get the equivalent density for calculating the transparency functions, which are further used to estimate the total nuclear reaction and differential elastic scattering cross sections, as discussed in Secs. III C and III D.

Some phenomenological parameters, related to the NN cross section, required to evaluate the profile function in Eq. (12) are σ_{NN}, α_{NN}, and β_{NN}, at different incident energies. In our calculation, these values are taken from Refs. [24,33], which are tabulated in Table V. Here, σ_{NN} stands for the total reaction cross section of NN collisions, α_{NN} is the ratio of the real to the imaginary part of the forward NN scattering amplitude, and β_{NN} is the slope parameter. The β_{NN} value estimates the fall of the angular distribution of the NN elastic scattering. It is to be noted that these parameters, in general, depend on the isospin of the nucleons (*pp, nn, pn*), and hence appropriate average values are obtained by interpolating a given set. The nucleon-nucleon cross section σ_{NN}, averaged over neutron and proton numbers, is calculated by the expression [24,34]

$$\bar{\sigma}_{NN}(E) = \frac{N_p N_t \sigma_{nn} + Z_p Z_t \sigma_{pp} + N_p Z_t \sigma_{np} + N_t Z_p \sigma_{np}}{A_p A_t}, \tag{18}$$

with Z_p, Z_t and N_p, N_t as the projectile and the target charge and neutron numbers, respectively. Note that σ_{NN} is the driving agent for the energy dependence of total reaction cross section σ_r, though, in view of the averages taken at each incident energy, the value of the input parameter σ_{NN} is not affected much by the neutron or proton number of the target and projectile system. This is a well-known feature of the total reaction cross section σ_r, and is thus relevant to recall.

TABLE III. Coefficients c_1, a_1 and c_2, a_2 of Gaussian functions, which are fitted to the density distributions generated from RMF(NL3) and E-RMF(G2) formalisms, for light nuclei (as projectiles).

Nucleus	RMF(NL3)				E-RMF(G2)			
	c_1	a_1	c_2	a_2	c_1	a_1	c_2	a_2
^{4}He	−1.05092	0.514949	1.24954	0.497397	−1.17133	0.509247	1.35243	0.490141
^{6}He	−1.1978	0.346115	1.41785	0.346236	−1.10191	0.364872	1.29553	0.356881
^{8}He	−1.19836	0.283782	1.41656	0.283924	−1.09579	0.325308	1.28739	0.313279
^{6}Li	−1.2017	0.338401	1.41367	0.338391	−1.20927	0.396482	1.39874	0.382147
^{7}Li	−1.10503	0.362372	1.31877	0.3517	−0.0246155	0.877594	0.2105	0.299145
^{8}Li	−1.18856	0.369719	1.4063	0.35237	−0.0483286	0.685948	0.235086	0.287981
^{9}Li	−0.029093	0.874689	0.245801	0.2808	−0.0788126	0.590314	0.266483	0.280958
^{11}Li	−0.0540616	0.628475	0.231925	0.231428	−0.0988483	0.51542	0.260122	0.237837
^{10}B	−0.145385	0.573468	0.379899	0.316861	−1.21283	0.394773	1.40704	0.353843
^{15}B	−0.299572	0.425976	0.480853	0.253374	−1.22064	0.3313	1.38249	0.284846
^{17}B	−0.224314	0.427336	0.396452	0.219516	−0.454951	0.344816	0.609667	0.236565
^{20}B	−0.180161	0.41492	0.339182	0.184949	−0.299283	0.341646	0.444999	0.197008
^{12}C	−0.232695	0.638683	0.517266	0.339919	−3.34808	0.379357	3.5471	0.359102
^{14}C	−3.77882	0.365346	3.96791	0.344481	−4.2207	0.347703	4.38557	0.330334
^{16}C	−1.32397	0.353965	1.50772	0.300361	−1.4157	0.336181	1.57637	0.289213
^{18}C	−0.610957	0.360143	0.785873	0.256258	−1.36173	0.312325	1.51661	0.266353
^{20}C	−0.522227	0.346399	0.687736	0.232099	−1.36876	0.291422	1.51713	0.247912

TABLE IV. Same as Table III, but for heavy nuclei (as targets).

Nucleus	RMF(NL3)				E-RMF(G2)			
	c_1	a_1	c_2	a_2	c_1	a_1	c_2	a_2
^{208}Pb	−2.64313	0.0532685	2.75724	0.0492428	−2.64946	0.0535256	2.766	0.0494824
^{210}Pb	−2.62315	0.0526782	2.73639	0.0486948	−2.65783	0.0531674	2.77348	0.0491542
^{218}Pb	−2.48912	0.0498046	2.59786	0.0460278	−2.79344	0.0515383	2.9102	0.0476675
^{228}Pb	−2.62604	0.0490159	2.73098	0.0453354	−2.66333	0.0494732	2.77043	0.0457665
^{248}Pb	−2.89059	0.0483861	2.99443	0.0447702	−2.59034	0.0458371	2.69484	0.0424171
^{260}Pb	−2.45222	0.0435363	2.56011	0.040285	−2.50225	0.0437805	2.6093	0.0405262
^{230}Th	−2.4835	0.047502	2.5857	0.043894	−2.54208	0.0479732	2.64437	0.0443404
^{240}Th	−2.67965	0.047258	2.77776	0.0437145	−2.6181	0.0468272	2.71599	0.0432986
^{250}Th	−2.74594	0.0464667	2.84506	0.0430046	−2.65942	0.0454064	2.75263	0.042005
^{270}Th	−2.74452	0.0462746	2.83967	0.0428277	−2.54056	0.042608	2.64133	0.0394314
^{235}U	−2.54853	0.0471019	2.64847	0.0435424	−2.54993	0.0471009	2.64931	0.0435372
^{238}U	−2.61151	0.0470922	2.71035	0.0435456	−2.58245	0.0467943	2.68049	0.0432664
^{250}U	−2.75588	0.046275	2.85145	0.0428272	−2.64917	0.0453065	2.74156	0.0419058
^{260}U	−2.456	0.0440042	2.56903	0.0407122	−2.694	0.0441555	2.78289	0.040853
^{270}U	−2.41462	0.0422599	2.52267	0.0390898	−2.62832	0.0429456	2.7238	0.039742
$^{292}X_{122}$	−3.30555	0.0435773	3.37668	0.0404026	−3.28593	0.043583	3.36194	0.0404295
$^{320}X_{122}$	−2.7657	0.0385546	2.85668	0.0357409	−2.69586	0.0383673	2.79456	0.0355931

TABLE V. Averaged nucleon-nucleon cross sections $\bar{\sigma}_{NN}$ (in fm^2) and other parameters used for the calculation of profile function at different incident energies (in MeV/nucleon).

Energy	30	49	85	100	120	150	200
$\bar{\sigma}_{NN}$	19.6	10.4	6.1	5.29	4.72	3.845	3.28
α_{NN}	0.87	0.94	1.0	1.435	1.38	1.245	0.93
β_{NN}	0.0	0.0	0.0	1.02	1.07	1.15	1.24
Energy	325	425	500	625	800	1100	2200
$\bar{\sigma}_{NN}$	3.03	3.025	3.62	4.0	4.26	4.32	4.335
α_{NN}	0.305	0.36	0.04	−0.095	−0.07	−0.275	−0.335
β_{NN}	0.62	0.48	0.125	0.16	0.21	0.22	0.26

TABLE VI. Total nuclear reaction cross sections, matter- and proton-distribution radii, obtained from RMF(NL3) and E-RMF(G2) formalisms and compared with experimental data [35] for various light projectiles on ^{12}C as target.

Projectile	σ_r (mb)			r_m (fm)			r_p (fm)		
	RMF	E-RMF	Expt.	RMF	E-RMF	Expt.	RMF	E-RMF	Expt.
^{20}Mg	1128.506	1198.646	1150(12)	2.858	2.883	2.86(3)	3.025	3.039	3.18(9)
^{20}Na	1125.769	1196.463	1094(11)	2.804	2.833	2.69(3)	2.902	2.926	3.14(5)
^{20}Ne	1148.289	1195.106	1144(10)	2.780	2.811	2.84(3)	2.798	2.828	3.10(7)
^{20}F	1124.297	1193.890	1113(11)	2.781	2.812	2.75(3)	2.700	2.737	2.98(4)
^{20}O	1125.730	1195.525	1078(10)	2.805	2.835	2.64(3)	2.599	2.642	2.72(5)
^{20}N	1132.357	1203.275	1121(17)	2.878	2.899	2.77(4)	2.538	2.587	2.39(20)

C. Total nuclear reaction cross sections

1. Total nuclear reaction cross sections with known experimental data

In our present calculation, we follow the procedure of the CSC_GM computer code [21]. In this method, the projectile nucleus is considered as a core plus a valence nucleon. For example, ^{11}Li nucleus is taken as the $^{10}\mathrm{Li} + 0p_{1/2}$-nucleon system. The present technique is very useful for loosely bound (exotic or drip line) nuclei, the projectile systems. Although the entire calculation is in the center-of-mass coordinate system, where there is no distinction between the projectile and the target, we use this terminology in order to distinguish them from one another. Throughout our calculation, in most cases, the lighter nucleus is a projectile and the heavier one a target nucleus.

After calculating the density profiles with RMF(NL3) and E-RMF(G2) methods, we estimate the coefficients of the Gaussian function and use them in the CSC_GM computer code [21] for evaluating the total nuclear reaction cross sections for some light nuclei (as projectiles) on ^{12}C (as the target in each case), where experimental measurements are available [35]. This is shown in Fig. 3 and Table VI. From Fig. 3, for $^{6,7,8,9,11}\mathrm{Li} + {}^{12}\mathrm{C}$ at 790 MeV/nucleon, it is clear that the E-RMF(G2) model overestimates slightly the measured total nuclear reaction cross section σ_r data, whereas the results obtained from the RMF(NL3) model agree well with the data. However, the halo nature of ^{11}Li is not reflected from Fig. 3, although an enhancement in total nuclear reaction cross section is evident for both the RMF(NL3) and E-RMF(G2) formalisms.

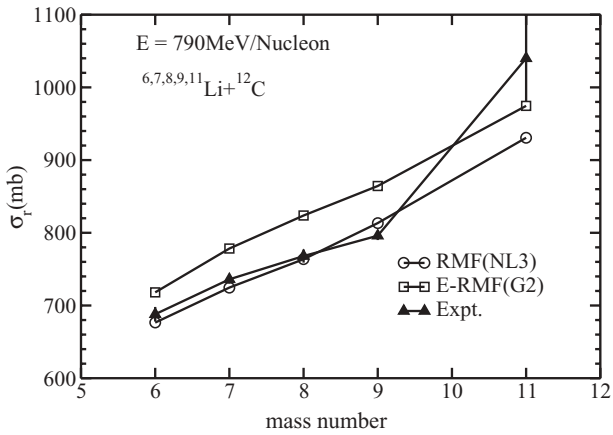

FIG. 3. Calculated total nuclear reaction cross sections σ_r as a function of the projectile mass, compared with the experimental data [35], for $^{6,7,8,9,11}\mathrm{Li} + {}^{12}\mathrm{C}$ reactions at 790 MeV/nucleon. The error bars in data are also shown.

In Table VI, we have compared our results of various other light projectiles on ^{12}C as the target, with the recently measured σ_r of Bochkarev *et al.* [35]. We notice that the experimental data lie in between the RMF(NL3) and E-RMF(G2) predictions. The RMF slightly underestimates the data, whereas the E-RMF overestimates marginally. For example, in the case of ^{20}Mg, the RMF underestimates the experimental data by 1.7% and the E-RMF overestimates it by about 4%. In other words, our calculations with respect to experimental data are quite convincing and can be extended to an unknown territory without the possibility of committing much error.

2. Total nuclear reaction cross sections for highly neutron-rich and superheavy nuclei

To measure the total reaction cross section for an unstable projectile with a stable target or an unstable target with a stable projectile or both as unstable nuclei is one of the challenging problems in experimental nuclear physics. As already mentioned in the Introduction, such measurements not only would provide a better understanding of the nuclear structure of such nuclei, but also are extremely useful for the formation of drip-line nuclei in many cosmological phenomena such as the x-ray bursts, GRBs, and supernovae explosions and in relativistic jets of GRBs or supernovae jets near the nascent neutron star, and in the r-process nucleosynthesis. To study such processes, in recent decades, considerable effort has been made to look for RIB+RIB cross sections at various laboratories [6]. In this context, it is worth studying such reaction processes, because understanding the mechanism of the formation of neutron-rich nuclei and the creation of superheavy elements is important not only in the cosmological systems but also in various laboratories of the world [36].

In some of our earlier work [26], it was shown that the Glauber model works remarkably well for RMF and E-RMF nuclear densities. The model reproduces experimental observables quite well for both the stable and unstable nuclei taken as targets and projectiles. In this paper, we extend

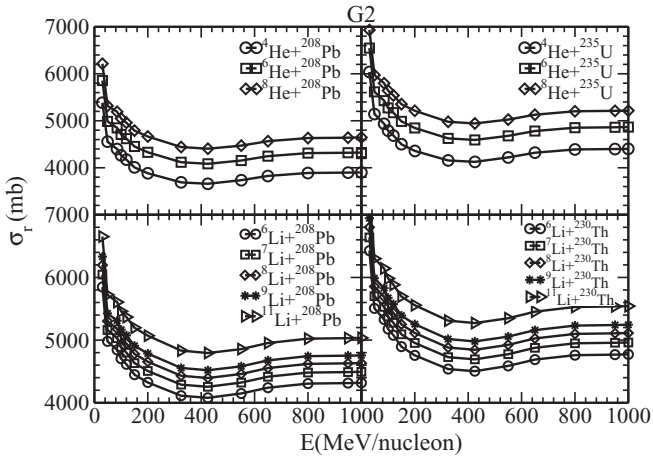

FIG. 4. Calculated total nuclear reaction cross sections for E-RMF(G2) formalism, taking He and Li isotopes as projectiles with different isotopes of Pb, Th, and U as targets.

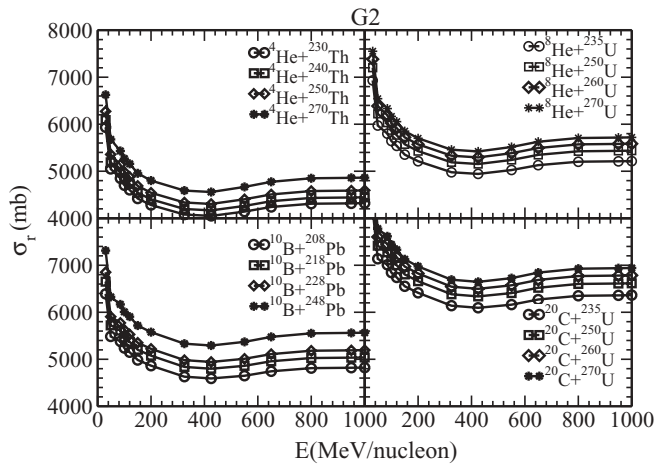

FIG. 6. Same as Fig. 4, but for He, B, and C isotopes as projectiles with different isotopes of Pb, Th, and U as targets.

the work of Ref. [26] to calculate the total nuclear reaction cross sections, using light mass isotopes as projectiles and heavy nuclei as targets. For heavier nuclei, we also use the neutron-rich thermally fissile nuclei (neutron-rich U and Th isotopes) which, as already stated in Sec. I, are more interesting from the point of view of energy production, not only in astrophysical systems but also in solving our future energy problems [37].

Figures 4–9 present our calculated total nuclear reaction cross sections for some selective stable-stable, stable-unstable, and unstable-unstable systems, such as He + Pb, He + U, He + Th, Li + Pb, Li + U, Li + Th, B + Pb, and C + U with different isotopes. Figures 4, 6, and 8 are for E-RMF(G2), and Figs. 5, 7, and 9 for RMF(NL3) formalism. First, we discuss the results with the E-RMF(G2) formalism.

Figure 4 shows the results of our calculation for different He and Li projectile masses with fixed targets as ^{208}Pb, ^{235}U, and ^{230}Th. In all of these cases, the total nuclear reaction cross section increases with the increase in mass of the projectile. At relatively lower incident energies (30–200 MeV/nucleon) of the projectile nucleus, the total nuclear reaction cross section is maximum, and it decreases rapidly with the increase of energy and, in all cases, a minimum in σ_r occurs at about 400 MeV/nucleon. As the incident energy is further increased, the total nuclear reaction cross section increases slightly and takes an almost constant value, which continues till the incident energy is 1000 MeV/nucleon. Note that in our calculations for heavier target masses, the medium modification is considered, which implies the probability of the formation of a heavier mass nucleus with the increase of mass number of the projectile as well as the target.

Figure 6 shows the total reaction cross sections for He, B, and C as projectiles with Th, U, Pb as targets. Unlike Fig. 4, here the projectile is fixed and the mass of the target changes. We find that here also the total nuclear reaction cross section increases with the increase of target mass. For example, σ_r for ^{270}Th is much more than the σ_r for ^{230}Th, with the same ^{4}He as projectile. Similarly, Fig. 8 demonstrates the results of our calculations for a fixed projectile with variable target masses in the cases of ^{6}Li + ^{208,218,228,248}Pb, ^{6}Li + ^{235,250,260,270}U, and ^{11}Li + ^{208,218,228,248}Pb, ^{11}Li + ^{235,250,260,270}U. Irrespective of a stable or unstable system, the total nuclear reaction cross section increases with increase of either the target mass

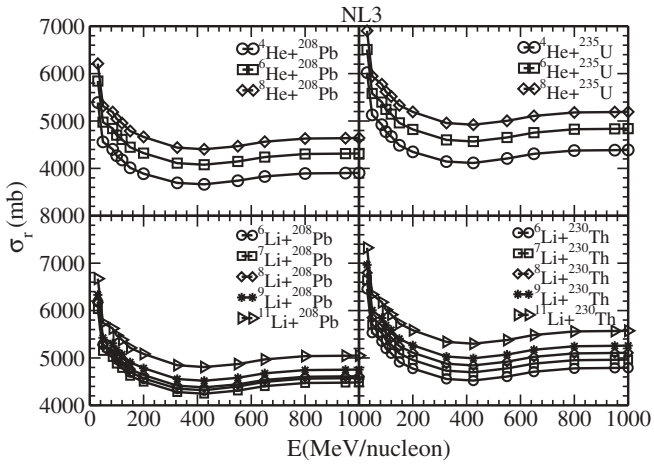

FIG. 5. Same as Fig. 4, but for RMF(NL3) formalism.

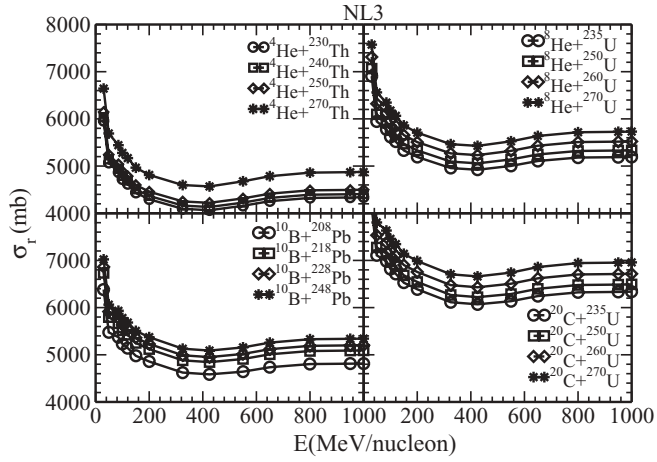

FIG. 7. Same as Fig. 6, but for RMF(NL3) formalism.

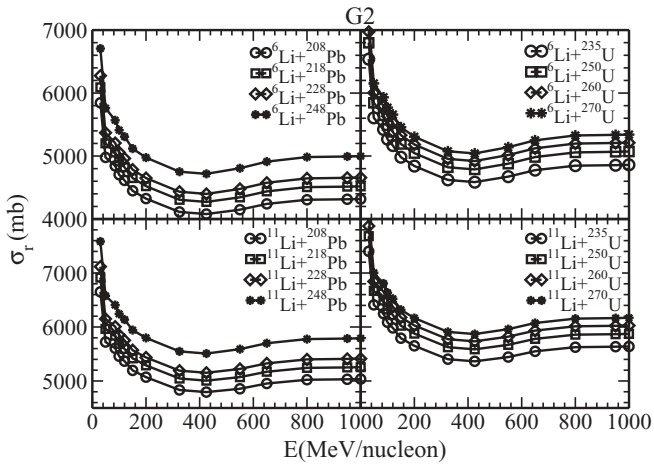

FIG. 8. Same as Fig. 4, but for Li nuclei as projectiles with different isotopes of Pb and U as targets.

A_t or the projectile mass A_p or both. This increase in total nuclear reaction cross section can be related to the geometrical area of the nucleus πR^2, where R is the sum of the radii of the target and the projectile nuclei. The nuclear radius is connected with the mass number of the nucleus via the relation $R = r_0 A^{1/3}$, where $r_0 = 1.36$ fm, and hence one expects $\sigma_r \propto (A_t^{1/3} + A_p^{1/3})^2$. Bradt and Peters [38] modified this relation to take into account the deviations from the experimental systematics and expressed it as $\sigma_r = \pi r_0^2 (A_t^{1/3} + A_p^{1/3} - b_0)^2$, with $b_0 = 2.247 - 0.915(A_p^{-1/3} - A_t^{-1/3})$. This formula is further improved in Ref. [39] and, later on, the Coulomb correction was also included [40]. The semiempirical formula for calculating the total nuclear reaction cross section [11,12] and experimental measurements [41] also show the size dependence of σ_r via the masses of target and projectile nuclei [41].

Summarizing the results of Figs. 4, 6, and 8 for some representative reactions, we find that the total nuclear reaction cross section increases with the increase of either the projectile or target mass or both. Also, the maximum value of σ_r occurs at a particular energy per nucleon, irrespective of the mass of the target or projectile. Interestingly, the same conclusions are

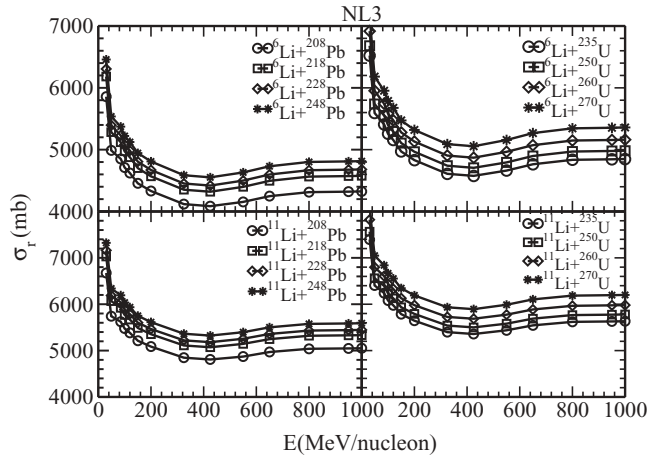

FIG. 9. Same as Fig. 8, but for RMF(NL3) formalism.

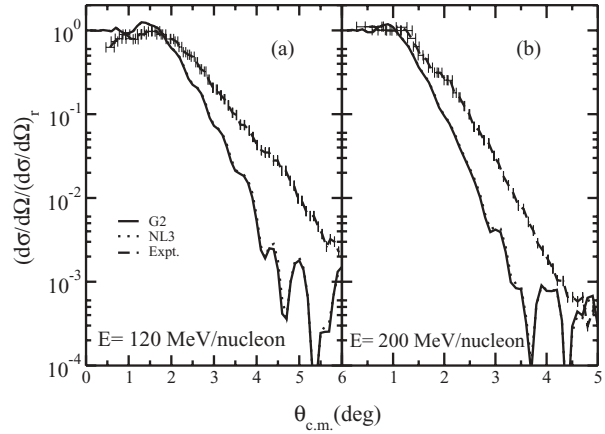

FIG. 10. Comparison of the experimental differential elastic scattering cross section with results of E-RMF(G2) and RMF(NL3) formalisms for ^{12}C + ^{208}Pb reaction at incident energies of (a) 120 and (b) 200 MeV/nucleon. The experimental data, shown with error bars, are from Ref. [45].

presented by Figs. 5, 7, and 9 for RMF(NL3), showing the force independence of the above results. From the behavior of our calculated total nuclear reaction cross section σ_r, the most important inference for the formation of superheavy elements that can be drawn is the following: from the increase in σ_r that occurs at a particular incident energy, we can conclude that the formation of a superheavy element is possible in some astrophysical accreting objects, such as the relativistic jets of γ-ray bursts (GRBs) or supernovae jets near the nascent neutron star [3,42–44].

D. Differential elastic scattering cross sections

Evaluation of the differential elastic scattering cross section $\frac{d\sigma}{d\Omega}$, defined in Eq. (15), is crucial to the study of scattering phenomenon. The results of our calculations for C + Pb, C + U, and Li + Pb systems at various incident energies are displayed in Figs. 10–14, and the extension of this calculation

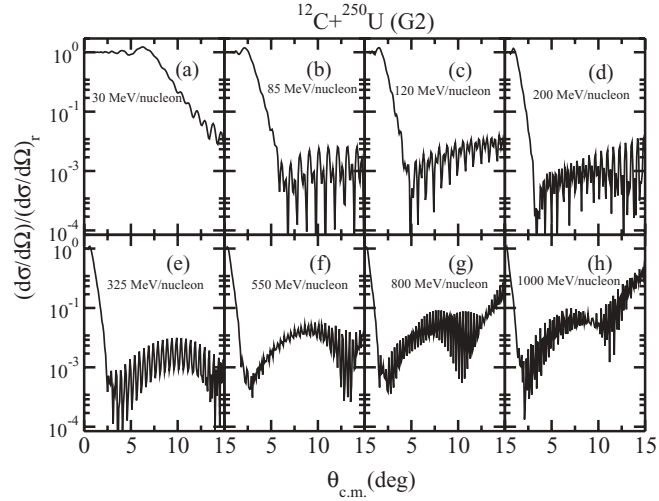

FIG. 11. Differential elastic scattering cross section for ^{12}C + ^{250}U at different energies, using the E-RMF(G2) formalism .

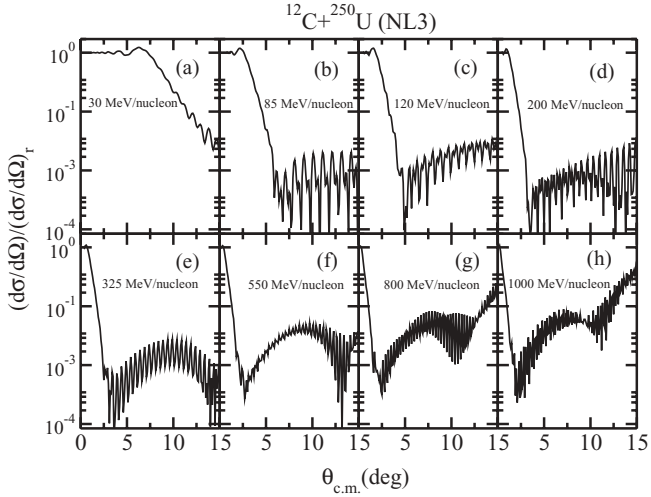

FIG. 12. Same as Fig. 11, but for the RMF(NL3) formalism.

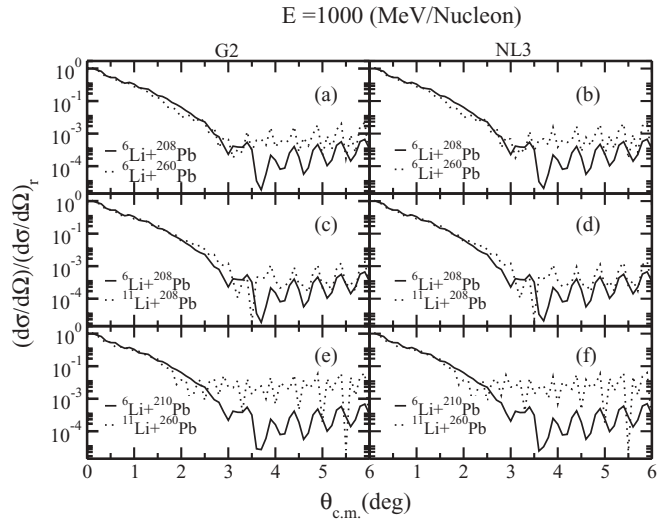

FIG. 14. Same as Fig. 13, but taking Li isotopes as projectiles with different isotopes of Pb nuclei as targets.

to the newly claimed to be discovered $^{292}X_{122}$ nucleus with the halo nucleus ^{11}Li taken as the projectile, in Fig. 15 in next subsection.

Figure 10 compares the calculated results with the experimental data [45] for the $^{12}C + ^{208}Pb$ system at two incident energies of 120 and 200 MeV/nucleon. Our calculations are carried out using both the E-RMF(G2) and RMF(NL3) formalisms, and they match the data reasonably well near the zero scattering angle. However, the discrepancy with the data increases as the scattering angle increases beyond a zero value. In general, the calculated $\frac{d\sigma}{d\Omega}$ for the two formalisms are similar and show a qualitative agreement with the data. A further inspection of Figs. 10(a) and 10(b) shows that the calculated differential elastic scattering cross sections provide a better agreement with the data at higher incident energy.

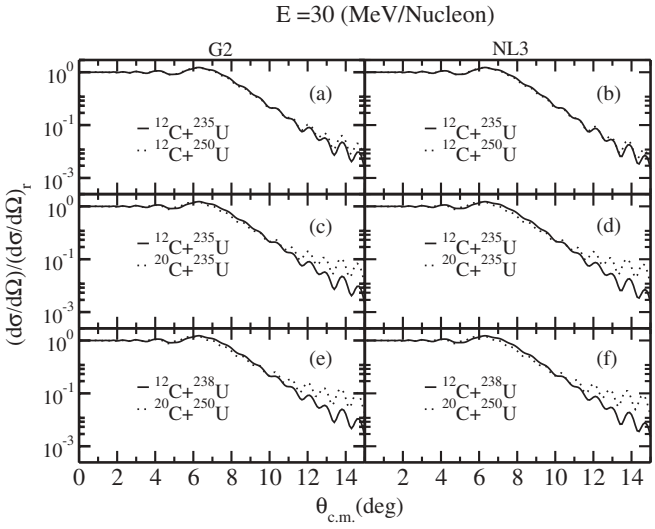

FIG. 13. Differential elastic scattering cross sections, taking C isotopes as projectiles with different isotopes of U nuclei as targets, for E-RMF(G2) (left) and RMF(NL3) (right) formalisms.

In other words, the calculated result is closer to the data for $E = 200$ than for $E = 120$ MeV/nucleon.

Figures 11 and 12 show similar calculations for the $^{12}C + ^{250}U$ system at the energies 30, 85, 120, 200, 325, 550, 800, and 1000 MeV/nucleon for, respectively, the E-RMF(G2) and RMF(NL3) densities. We notice in Figs. 11 and 12 that the differential elastic scattering cross sections for the system $^{12}C + ^{250}U$ show a large variation with incident energy. Interestingly, the results obtained by using the two formalisms, E-RMF(G2) and RMF(NL3), are almost identical, and hence force-independent, for the entire energy range of 30–1000 MeV/nucleon over the large spectrum of angular distribution, starting from 0° up to 15°. The typical, Fresnel type, diffraction effect appears in the small-angle region (5°–10° for C+U system at 30 MeV/nucleon), which is due to the interference of Coulomb and nuclear amplitudes. On the other hand, the oscillatory behavior of the elastic scattering cross section at large scattering angles, as well as at higher incident energy per nucleon, could possibly be an artifact of some numerical instability of our calculations. However, we have thoroughly checked our calculations for the various inputs, such as the number of points in the Monte Carlo integration method, etc., and find that the observed oscillations are perhaps real.

Figures 13 and 14 give our results for some selected cases at two incident energies of 30 and 1000 MeV/nucleon. The systems chosen at 30 MeV/nucleon are ($^{12}C + ^{235}U$, $^{12}C + ^{250}U$), ($^{12}C + ^{235}U$, $^{20}C + ^{235}U$), and ($^{12}C + ^{238}U$, $^{20}C + ^{250}U$); and at 1000 MeV/nucleon are ($^{6}Li + ^{208}Pb$, $^{6}Li + ^{260}Pb$), ($^{6}Li + ^{208}Pb$, $^{11}Li + ^{208}Pb$), and ($^{6}Li + ^{210}Pb$, $^{11}Li + ^{260}Pb$). Apparently, in Fig. 13, the differential elastic scattering cross section for C isotopes with different masses of U nuclei at 30 MeV/nucleon of the projectile energy constitute cases of stable+unstable, unstable+stable, stable+stable, and unstable+unstable projectile-target systems. The left panel of the figure is for E-RMF(G2) and right one for RMF(NL3). We notice in Fig. 13 that, for all cases, the $\frac{d\sigma}{d\Omega}$ is similar in magnitude for both the stable and unstable systems at small scattering

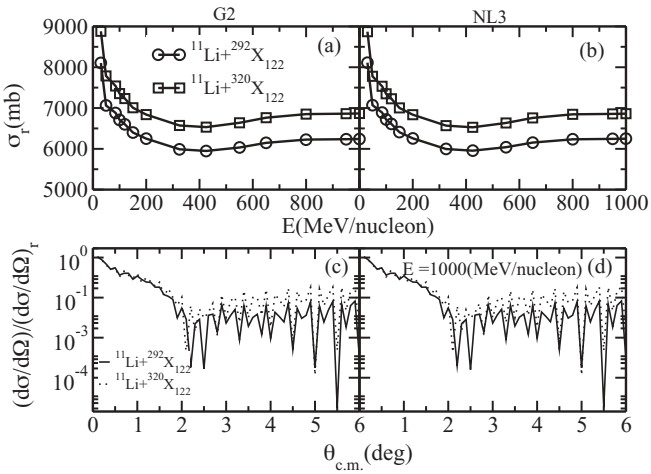

FIG. 15. Total nuclear reaction cross sections and differential elastic scattering cross sections, for ^{11}Li taken as the projectile with the isotopes $^{292,320}X_{122}$ as targets.

angles. However, a significant increase in the differential elastic scattering cross section appears for heavier isotopes with the increase of scattering angle θ. This phenomenon is more conspicuous for high-energy scattering, as shown in Fig. 14 for different combinations of Li and Pb nuclei.

E. Applications to recently discovered superheavy elements

As already mentioned in the Introduction, recently, the superheavy nucleus with $Z = 122$ or 124 and mass number $A = 292$ has possibly been discovered in natural Th [5]. The estimated half-life of this isotope is $T_{1/2} \geqslant 10^8$ yr, which is in good agreement with various theoretical predictions [46,47]. Therefore, taking this newly discovered nucleus as a target, it is interesting to study the total nuclear reaction and differential elastic scattering cross sections, with a highly neutron-rich nucleus like ^{11}Li as the projectile.

Figure 15 shows the σ_r and $\frac{d\sigma}{d\Omega}$ for the systems $^{11}\mathrm{Li} + {}^{292}X_{122}$ and $^{11}\mathrm{Li} + {}^{320}X_{122}$, using both the E-RMF(G2) and RMF(NL3) methods. We notice from this figure that, just as before, σ_r increases with mass of the target, and the magnitude of $\frac{d\sigma}{d\Omega}$ decreases with scattering angle (up to $\theta = 2^\circ$) and ends in vigorous oscillations (maxima-minima) [see Figs. 15(c) and 15(d)]. The above result is irrespective of the formalism used. In fact, the scenario for differential elastic scattering cross section resembles the phenomenon already observed above for the known heavy elements such as Pb and U in Figs. 10 and 11.

IV. SUMMARY

We have used the Glauber model for calculating the total nuclear reaction cross sections with densities obtained from RMF and E-RMF formalisms. After showing that the calculations of total nuclear reaction cross sections performed with the Glauber model, using RMF and E-RMF nuclear densities as the ingredients, match the measured data nicely, we have extended its application to the recently predicted neutron-rich, thermally fissile uranium and thorium isotopes. We have shown that the total nuclear reaction cross sections decrease with the increase of incident energy of the projectile. In most cases, the neutron-rich light mass nuclei are used as projectiles and heavy nuclei as targets. To see the effect of the neutron richness of the projectile in the exotic mass region, we repeated the calculations with various projectile masses without changing the target nucleus. We found that the total nuclear reaction cross section increases with increase of the projectile mass or with increase of neutron number of the target. Such a result is valid for both the normal and neutron-rich nuclei. Thus, our framework seems ideal for the simple analysis of the different ranges of data on total nuclear reaction cross sections of neutron-rich unstable nuclei. However, unlike the total nuclear reaction cross sections, the differential elastic scattering cross sections show marginal changes with the change of projectile mass, exclusively in the vicinity of the zero scattering angle.

ACKNOWLEDGMENTS

This work has been supported in part by the Council of Scientific & Industrial Research [No. 03(1060)06/EMR-II], as well as the Department of Science and Technology, Government of India, Project No. SR/S2/HEP-16/2005.

[1] A. Ozawa, T. Suzuki, and I. Tanihata, Nucl. Phys. **A693**, 32 (2001).
[2] F. M. Nunes, N. C. Summers, A. M. Moro, and A. M. Mukhamedzhanov, in Proceedings of "Nuclei at the Limits," ANL 26–30 July 2004, arXiv:nucl-th/0505046.
[3] S. K. Patra and R. N. Panda, arXiv:0906.3797v1 [nucl-th].
[4] L. Satpathy, S. K. Patra, and R. K. Choudhury, PRAMANA J. Phys. **70**, 87 (2008).
[5] A. Marinov, I. Rodushkin, D. Kolb, A. Pape, Y. Kashiv, R. Brandt, R. V. Gentry, and H. W. Miller, arXiv:0804.3869 [nucl-ex]; S. K. Patra, M. Bhuyan, M. S. Mehta, and R. K. Gupta, Phys. Rev. C **80**, 034312 (2009).
[6] I. Tanihata, J. Phys. G: Nucl. Part. Phys. **22**, 157 (1996).
[7] P. G. Hansen and B. Jonson, Europhys. Lett. **4**, 409 (1989).
[8] R. J. Furnstahl, B. D. Serot, and H. B. Tang, Nucl. Phys. **A615**, 441 (1997); R. J. Furnstahl and B. D. Serot, *ibid.* **A671**, 447 (2000).
[9] P. Arumugam, B. K. Sharma, P. K. Sahu, S. K. Patra, T. Sil, M. Centelles, and X. Viñas, Phys. Lett. **B601**, 51 (2004).
[10] S. Kox *et al.*, Phys. Rev. C **35**, 1678 (1987).
[11] H. P. Wellisch and D. Axen, Phys. Rev. C **54**, 1329 (1996).
[12] C.-T. Liang, Y.-A. Luo, X.-H. Li, and C.-H. Cai, J. Phys. G: Nucl. Part. Phys. **36**, 015102 (2009).
[13] L. Sihver, C. H. Tsao, R. Silberberg, T. Kanai, and A. F. Barghouty, Phys. Rev. C **47**, 1225 (1993).
[14] S. K. Patra and C. R. Praharaj, Phys. Rev. C **44**, 2552 (1991); Y. K. Gambhir, P. Ring, and A. Thimet, Ann. Phys. (NY) **198**, 132 (1990).

[15] M. Del Estal, M. Centelles, X. Viñas, and S. K. Patra, Phys. Rev. C **63**, 044321 (2001); M. Del Estal, M. Centelles, X. Viñas, and S. K. Patra, *ibid.* **63**, 024314 (2001); S. K. Patra, M. Del Estal, M. Centelles, and X. Viñas, *ibid.* **63**, 024311 (2001).
[16] B. D. Serot and J. D. Walecka, Int. J. Mod. Phys. E **6**, 515 (1997).
[17] R. J. Furnstahl, B. D. Serot, and H. B. Tang, Nucl. Phys. **A598**, 539 (1996).
[18] G. A. Lalazissis, J. König, and P. Ring, Phys. Rev. C **55**, 540 (1997).
[19] R. J. Glauber, in *Lectures on Theoretical Physics*, edited by W. E. Brittin and L. C. Dunham (Interscience, New York, 1959), Vol. 1, p. 315.
[20] J. Chauvin, D. Lebrun, A. Lounis, and M. Buenerd, Phys. Rev. C **28**, 1970 (1983); M. Buenerd, A. Lounis, J. Chauvin, D. Lebrun, P. Martin, G. Duhamel, J. C. Gondrand, and P. D. Saintignon, Nucl. Phys. **A424**, 313 (1984).
[21] B. Abu Ibrahim, Y. Ogawa, Y. Suzuki, and I. Tanihata, Comput. Phys. Commun. **151**, 369 (2003).
[22] P. Shukla, Phys. Rev. C **67**, 054607 (2003).
[23] A. Bhagwat and Y. K. Gambhir, Phys. Rev. C **77**, 027602 (2008); **73**, 054601 (2006); **73**, 024604 (2006); **69**, 014315 (2004); **68**, 044301 (2003).
[24] P. J. Karol, Phys. Rev. C **11**, 1203 (1975).
[25] J. P. Blaizot, Phys. Rep. **64**, 171 (1980).
[26] A. Shukla, B. K. Sharma, R. Chandra, P. Arumugam, and S. K. Patra, Phys. Rev. C **76**, 034601 (2007); B. K. Sharma, S. K. Patra, R. K. Gupta, A. Shukla, P. Arumugam, P. D. Stevenson, and W. Greiner, J. Phys. G: Nucl. Part. Phys. **32**, 2089 (2006).
[27] G. Audi, A. H. Wapstra, and C. Thibault, Nucl. Phys. **A729**, 337 (2003).
[28] P. Möller *et al.*, Phys. Rev. Lett. **99**, 252501 (2007).
[29] G. Ewald *et al.*, Phys. Rev. Lett. **93**, 113002 (2004).
[30] R. Sanchez *et al.*, Phys. Rev. Lett. **96**, 033002 (2006).
[31] C. W. De Jager, H. De Vries, and C. DeVries, At. Data Nucl. Data Tables **14**, 479 (1974).
[32] Y. Ogawa, K. Yabana, and Y. Suzuki, Nucl. Phys. **A543**, 722 (1992); J. N. De, X. Viñas, S. K. Patra, and M. Centelles, Phys. Rev. C **64**, 057306 (2001).
[33] M. Y. H. Farag, Eur. Phys. J. A **12**, 405 (2001).
[34] S. K. Charagi and S. K. Gupta, Phys. Rev. C **41**, 1610 (1990); S. K. Charagi, *ibid.* **48**, 452 (1993); S. K. Charagi and S. K. Gupta, *ibid.* **46**, 1982 (1992); **56**, 1171 (1997).
[35] O. V. Bochkarev *et al.*, Eur. Phys. J. A **1**, 15 (1998).
[36] Yu. Ts. Oganessian *et al.*, Phys. Rev. C **74**, 044602 (2006); **79**, 024608 (2009); **79**, 024603 (2009); **76**, 011601(R) (2007).
[37] See, e.g., http://www.nature.com/nindia/2008/080520/full/nindia.2008.204.html, as highlighted in *Nature India*, 20 May (2008).
[38] L. H. Bradt and B. Peters, Phys. Rev. **77**, 54 (1950).
[39] S. Barshay, C. B. Dover, and J. P. Vary, Phys. Rev. C **11**, 360 (1975); Phys. Lett. **B51**, 5 (1974).
[40] A. Ingemarsson and M. Lantz, Phys. Rev. C **67**, 064605 (2003); **72**, 064615 (2005).
[41] J. Y. Hostachy *et al.*, Nucl. Phys. **A490**, 441 (1988); V. Bernard *et al. ibid.* **A423**, 511 (1984).
[42] P. A. Mazzali, J. Deng, K. Nomoto, D. N. Sauer, E. Pian, N. Tominaga, M. Tanaka, K. Maeda, and A. V. Filippenko, Nature (London) **442**, 1018 (2006).
[43] T. A. Thompson, P. Chang, and E. Quataert, Astrophys. J. **611**, 380 (2004).
[44] P. O. Lagage and C. J. Cesarsky, Astron. Astrophys. **125**, 249 (1983).
[45] B. Bonin, J. Physique **48**, 1479 (1987).
[46] S. G. Nilsson, J. R. Nix, A. Sobiczewski, Z. Szymanski, S. Wycech, C. Gustafson, and P. Möller, Nucl. Phys. **A115**, 545 (1968); S. G. Nilsson, C. F. Tsang, A. Sobiczewski, Z. Szymanski, S. Wycech, C. Gustafson, I.-L. Lamm, P. Möller, and B. Nilsson, *ibid.* **A131**, 1 (1969).
[47] M. Brack, J. Damgaaid, A. S. Jensen, H. C. Pauli, V. M. Strutinsky, and C. Y. Wong, Rev. Mod. Phys. **44**, 320 (1972); E. O. Fiset and J. R. Nix, Nucl. Phys. **A193**, 647 (1972); J. R. Nix, Annu. Rev. Nucl. Sci. **22**, 65 (1972).